Influence of Network Topology on the Elasticity of the Red Blood Cell Membrane Skeleton

J. C. Hansen*, R. Skalak,*# S. Chien*, and A. Hoger*#
*Department of Bioengineering, and #Department of Applied Mechanics and Engineering Sciences, Division of Mechanical Engineering, University of California, San Diego, La Jolla, California 92093 USA

ABSTRACT A finite-element network model is used to investigate the influence of the topology of the red blood cell membrane skeleton on its macroscopic mechanical properties. Network topology is characterized by the number of spectrin oligomers per actin junction (ϕ_a) and the number of spectrin dimers per self-association junction (ϕ_s). If it is assumed that all associated spectrin is in tetrameric form, with six tetramers per actin junction (i.e., $\phi_a = 6.0$ and $\phi_s = 2.0$), then the topology of the skeleton may be modeled by a random Delaunay triangular network. Recent images of the RBC membrane skeleton suggest that the values for these topological parameters are in the range of $4.2 < \phi_a < 5.5$ and $2.1 < \phi_s < 2.3$. Model networks that simulate these realistic topologies exhibit values of the shear modulus that vary by more than an order of magnitude relative to triangular networks. This indicates that networks with relatively sparse nontriangular topologies may be needed to model the RBC membrane skeleton accurately. The model is also used to simulate skeletal alterations associated with hereditary spherocytosis and Southeast Asian ovalocytosis.

INTRODUCTION

The red blood cell (RBC) membrane skeleton is a highly deformable network, composed mainly of spectrin, that reinforces the cytoplasmic face of the RBC membrane. The head ends of spectrin dimers are linked together by spectrin self-association, and the tail ends bind to junctions containing short actin filaments and other skeletal proteins. In normal RBCs, the skeleton enables the cell to undergo large extensional deformations while maintaining the structural integrity of the membrane. Abnormal RBCs with various alterations of skeletal structure can exhibit either an increase or a decrease in membrane stiffness, resulting in impaired cellular function. The link between skeletal microstructure and membrane mechanical properties has been well documented by genetic (e.g., Palek and Jarolim, 1993) and physiochemical (e.g., Deuticke et al., 1990) alterations of the RBC skeleton. Two structural features that affect membrane mechanical properties are the intrinsic elasticity of spectrin and the geometric organization (topology) of spectrin molecules within the skeleton.

Several quantitative models of the RBC membrane have been proposed that assume spectrin elasticity is of entropic origin and predict the mechanical properties of the skeleton in terms of gel-like elasticity (Stokke et al., 1986; Kozlov and Markin, 1987; Boal, 1994). These models generally neglect the presence of spectrin hexamers. We have taken a different computational approach that allows the consideration of a variety of assumptions about the topology of the skeleton and the intrinsic elasticity of spectrin (Hansen et al., 1996). Specifically, we construct random two-dimensional networks in which each edge (or spring element) corresponds to a spectrin molecule, and nodes represent protein junctions in the RBC membrane skeleton. These networks are subjected to a series of deformations for which the resulting stresses and strains are computed by finite-element model (FEM) analysis, and are then used to characterize the properties of the discrete model network in terms of the shear modulus (μ) and the area expansion modulus (κ) of an equivalent isotropic, nonlinear two-dimensional continuum. These computational procedures were introduced and implemented by Hansen et al. (1996).

In this paper we study the influence of skeletal topology on RBC membrane elasticity. Previous models of RBC skeletal structure have typically been based on the assumption that all spectrin is in the form of a tetramer, but more recent data indicate that hexamers may comprise a relatively large fraction of spectrin in the native RBC skeleton. Therefore, we construct networks that contain some Y-shaped triads of elements corresponding to hexamers.

Reported values for topological parameters of the RBC membrane skeleton vary significantly with the method of sample preparation and visualization. For the range of topologies that have been observed, we construct networks with equivalent topological parameters and compute the elastic moduli of these networks by FEM analysis. Within this range of topologies, we find that the computed values of μ/K and κ/K vary by more than an order of magnitude, indicating that skeletal topology is an important determinant of RBC membrane elasticity.

Our modeling approach is also used to investigate a variety of genetic defects of RBC skeletal proteins that are known to induce changes in both the topology of the skeleton and the shear elasticity of the RBC membrane. Abnormal skeletal topologies are incorporated into our model by

Received for publication 12 March 1996 and in final form 19 February 1997.

Address reprint requests to Dr. Anne Hoger, Department of Applied Mechanics and Engineering Sciences, University of California, San Diego, La Jolla, CA 92093-0411. Tel.: 619-534-2169; Fax: 619-534-5698; E-mail: ahoger@ames.ucsd.edu.

0006-3495/97/05/2369/13 $2.00

altering the connectivity of springs in a random network. For each type of topological abnormality, the model is evaluated by comparing our predicted values (μ) with measured values of the shear modulus (μ_m) for RBCs with that defect.

One type of topological variation that we consider is caused by a reduction in spectrin content. Skeletons that are deficient in spectrin and exhibit a relatively sparse topology are modeled by randomly removing elements from a network. For such networks, our model predicts a decrease in μ that is similar to the decrease in μ_m of spectrin-deficient RBCs in hereditary spherocytosis (HS). RBC skeletal topology may also be altered by an increase in spectrin connectivity. This type of alteration is modeled by randomly inserting cross-linking elements in a network. Our results resemble the increase in stiffness that has been observed for RBCs in Southeast Asian ovalocytosis (SAO).

TOPOLOGY OF THE NORMAL RBC MEMBRANE SKELETON

The primary structural component of the RBC membrane skeleton is spectrin, a highly extensible elastic molecule. The ends of spectrin dimers are linked together by spectrin self-association and by junctional complexes containing actin and protein 4.1, shown schematically in Fig. 1. Band 3 is a transmembrane protein that serves as a major site of skeletal attachment to the lipid bilayer through interactions with ankyrin and protein 4.2 (e.g., Shen, 1989; Chien and Sung, 1990; Bennett and Gilligan, 1993).

The topology of the RBC membrane skeleton can be characterized in terms of two parameters: 1) the number of spectrin dimers per self-association junction (ϕ_s), which is related to the relative amounts of spectrin oligomers, and 2) the average number of spectrin oligomers joined to each actin junction (ϕ_a). Values for these parameters have been measured by biochemical methods and by visualization of the skeleton, with some parameters varying significantly among the different approaches.

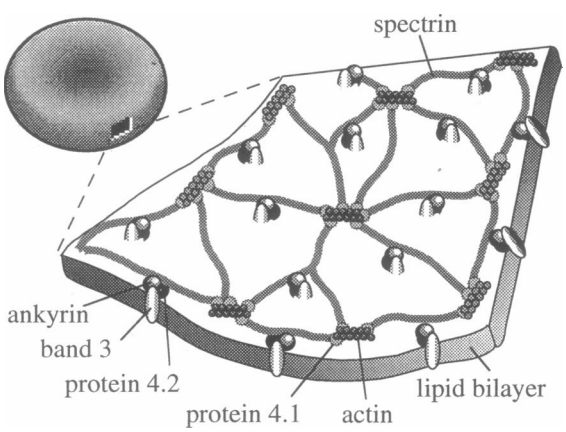

FIGURE 1 Arrangement of the major components of the RBC membrane skeleton.

Relative amounts of oligomeric forms of spectrin

A spectrin dimer is composed of one α subunit and one β subunit, which form an antiparallel pair of intertwined strands, each of which is an α-helical triple-coiled coil with 18–20 homologous repeating regions (Speicher and Marchesi, 1984; Parry et al., 1992; Yan et al., 1993). The head ends of spectrin dimers (SpD) can self-associate to form tetramers (SpT), hexamers (SpH), octamers (Sp8), and higher order oligomers (see Fig. 2) (Morrow and Marchesi, 1981). When spectrin is extracted from the RBC membrane at low temperatures (0–5°C), dissociation and reassociation are inhibited. Therefore the distribution of spectrin oligomers in such extracts (as measured by gel densitometry) is considered to be representative of the state of spectrin in the native skeleton. In extracts of normal RBCs, 5–10% of the total mass of spectrin is in SpD form, 45–55% is in SpT form, and 25–35% is present as SpH or higher order oligomers (Liu et al., 1984).

A different distribution of spectrin oligomers is observed in images of the RBC membrane skeleton obtained by electron microscopy (EM). A primary difference from the gel electrophoretic finding is the absence of SpD in these images. It is not known whether the "missing" dimers undergo self-association in the skeleton, form globular clusters, or simply become detached from the skeleton during sample preparation (Coetzer et al., 1990; Liu et al., 1990a). The proportion of Sp8 and higher order oligomers is also less than expected in EM images of the skeleton. In any case, visualization techniques can generally be used to measure the relative amounts of SpT and SpH, but not other oligomeric forms of spectrin.

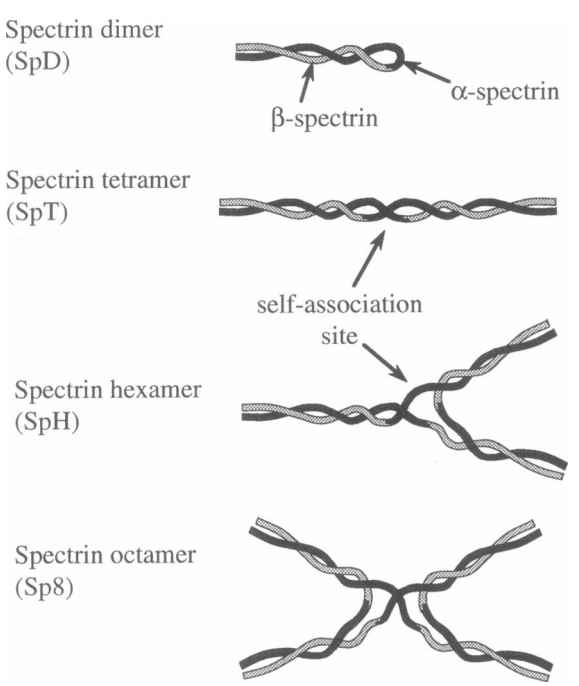

FIGURE 2 Interaction of α-spectrin and β-spectrin in a dimer (SpD), tetramer (SpT), hexamer (SpH), and octamer (Sp8).

When RBC membrane skeletons are removed from the lipid bilayer and fully expanded in low ionic strength solutions, the individual components of the skeleton may be resolved by negative staining EM. These skeletons resemble random triangular networks, and most of the spectrin (84% of oligomers) appears to be present in the form of a tetramer (Byers and Branton, 1985; Liu et al., 1987). Similar results have been obtained by visualizing skeletons with varying degrees of spreading (Shen et al., 1986; McGough and Josephs, 1990; Derick et al., 1992). Unspread and partially spread skeletons have been prepared for EM with a quick-freeze, deep-etch, rotary replication (QFDERR) technique. In these images, the proportion of hexamers is estimated to be as high as 30–40% (Ursitti et al., 1991; Ursitti and Wade, 1993). It has been proposed that the fraction of SpH may be artifacturally reduced in images of spread skeletons (Ursitti and Wade, 1993). Visualization data are often reported as %SpT or %SpH among oligomers of spectrin, unlike densitometry data, which report the percentage of spectrin mass that is present in a particular form. Therefore, to permit comparison of these measurements, results are expressed in terms of the mass ratio SpT/(SpT + SpH). The values, obtained by various methods, are summarized in Table 1.

In our model, unassociated SpD's are not included, because elements must form connections at both ends to make a structural contribution to the network. Higher order oligomers such as Sp8 are rare, so they are also neglected. Therefore, to construct model networks that mimic the topology of the RBC membrane skeleton, we assume that the skeleton contains only tetramers and hexamers (Fig. 2). The relative amounts of SpT and SpH are characterized in terms of the parameter ϕ_s, which is defined as the average number of spectrin dimers bound to each self-association site. A value of $\phi_s = 2.0$ indicates that 100% of the spectrin is in the SpT form, and $\phi_s = 3.0$ means that 100% of the spectrin is in the SpH form. As shown in Table 1, we consider values for ϕ_s of ~2.1–2.3.

Average number of spectrin dimers per actin junction

RBC skeletal topology is also affected by the average number of spectrin molecules per actin junction, ϕ_a. Each actin junction, containing 12–14 monomers of actin, is expected to be able to bind four to seven spectrin dimers (Gilligan and Bennett, 1993). This estimate is generally consistent with the number of spectrin molecules per actin junction observed in EM images of the RBC membrane skeleton. In electron micrographs of spread, negatively stained skeletons, the average number of spectrin molecules per actin junction is between 4.9 and 5.5 (Table 2). When partially spread skeletons are not subjected to negative staining, but are prepared by the QFDERR technique instead, then the average number of spectrins per actin junction is lower: $\phi_a = 4.2 \pm 0.7$ (Ursitti and Wade, 1993).

In summary, EM images of partially spread skeletons prepared by QFDERR show average values of $\phi_s = 2.3$ and $\phi_a = 4.2$. When skeletons are spread and negatively stained before EM visualization, the average values observed are $\phi_s = 2.1$ and $\phi_a = 4.9$–5.5. In either case, the topology of the RBC membrane skeleton differs from the topology of a triangular network ($\phi_s = 2.0$ and $\phi_a = 6.0$).

TOPOLOGICAL ALTERATIONS OF THE RBC MEMBRANE SKELETON

In subsequent sections, our model is used to simulate defects in skeletal topology, predict changes in the shear modulus for such networks, and compare the results with experimental data. Two particular diseases, hereditary spherocytosis and Southeast Asian ovalocytosis, have been chosen because their underlying defects are relatively well characterized at the molecular level, and the resulting changes in intrinsic membrane elasticity have been measured experimentally by the micropipette aspiration technique.

Hereditary spherocytosis

Hereditary spherocytosis (HS) is a form of hereditary hemolytic anemia that is characterized by the presence of abnormally small and round erythrocytes in peripheral blood smears. These changes in RBC shape result from a deficiency of spectrin, which is believed to induce a compensatory lipid removal mechanism that partially restores the normal density of spectrin in the skeleton (Becker and Lux, 1985; Liu et al., 1990b). A spectrin deficiency typi-

TABLE 1 Relative amounts of several oligomeric forms of spectrin, as measured by gel densitometry and visualization of RBC membrane skeletons by electron microscopy

		SpD	SpT	SpH	≥Sp8	$\frac{\text{SpT}}{(\text{SpT} + \text{SpH})}$	ϕ_s
Gel densitometry (Liu et al., 1984)	% mass	8	52	14	15	0.79	2.15
EM, fully spread, negatively stained (Liu et al., 1987)	% oligomers	—	84	11	5		
	% mass	—	76	15	9	0.84	2.1
EM, partially spread QFDERR (Ursitti and Wade, 1993)	% oligomers	—	68	30	2		
	% mass	—	58	38	3	0.60	2.3

TABLE 2 Average number of spectrin molecules per actin junction (ϕ_a), and the range of values obtained for the number of spectrin molecules joined to a particular actin junction by different experimental methods

Method	ϕ_a	Range	Reference
EM, fully spread and negatively stained	—	5–7	Liu et al. (1987)
	5.0–5.5	3–7	Liu et al. (1990a)
EM, partially spread and negatively stained	5.3	4–7	Byers and Branton (1985)
	—	5–8	Shen et al. (1986)
	4.9	2–6	Ursitti and Wade (1993)
EM, partially spread, by QFDERR	4.2 ± 0.7	2–6	Ursitti and Wade (1993)

cally arises as a secondary effect of abnormal association of spectrin with other skeletal proteins, such as ankyrin, protein 4.1, band 3, and protein 4.2 (see, e.g., Palek and Jarolim, 1993). The degree of spectrin deficiency in HS is often quantified in terms of the ratio of spectrin to band 3 (Sp/b3). In normal RBCs, Sp/b3 $\approx$ 1.0. In RBCs of HS patients, values for Sp/b3 vary and can be as low as 0.4 (Liu et al., 1990a; Savvides et al., 1993).

The structural organization of the RBC skeletons of HS patients has been observed by EM of spread, negatively stained skeletons. As spectrin content decreases, the network becomes sparse, with a reduction of ϕ_a that can be as low as $\phi_a = 3.3$ in skeletons with a severe spectrin deficiency (Liu et al., 1990a). ϕ_a appears to vary linearly with Sp/b3, or equivalently, with the total number of dimers available for binding in the skeleton (N_d). The number of spectrin molecules per actin junction is defined by the ratio $\phi_a = N_d/N_a$, where N_a is the number of actin junctions in the network (see Appendix). Because the measured values for ϕ_a and N_d vary proportionately, this relationship indicates that N_a is essentially constant. For purposes of our analysis, we assume that the major topological change in HS skeletons is a decrease in ϕ_a, due to a reduction in the number of spectrin linkages, whereas the number of actin junctions remains the same (see Fig. 3, *a* and *b*). This assumption is also supported by EM images of intact skeletons prepared by QFDERR, which indicate that the number of junctions containing four or more molecules (presumably spectrin) is reduced in HS skeletons (Ohno et al., 1993).

The membrane shear modulus (μ_m) of spectrin-deficient RBCs, as measured by micropipette aspiration, is reduced relative to μ_m of normal RBCs. The decrease in μ_m correlates with the reduction in Sp/b3 (Waugh, 1987; Waugh and Agre, 1988). As spectrin is removed from the membrane and Sp/b3 decreases from 1 to approximately 0.7, the shear modulus decreases proportionately. For Sp/b3 between 0.7 and 0.4, the shear modulus remains constant at about 60% of its normal value (Waugh and Agre, 1988). Human RBCs with Sp/b3 below 0.4 are rare, and extremely fragile, so reliable mechanical measurements are not available for such cells.

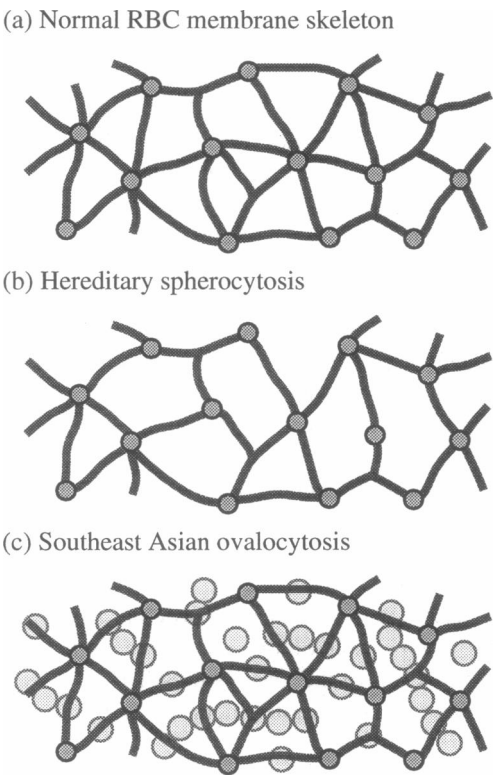

FIGURE 3 Schematic drawings of variations in RBC skeletal topology. (*a*) Normal RBCs. Thick lines represent SpT and SpH, and small circles correspond to actin junctions. (*b*) Spectrin deficiency in HS. (*c*) Formation of band 3 aggregates in SAO. Large circles indicate the positions of mutant band 3 in the membrane.

Southeast Asian ovalocytosis

Southeast Asian ovalocytosis (SAO) is an asymptomatic variation of hereditary elliptocytosis (HE) that is highly prevalent (up to 30% of the population) in certain parts of Malaysia and Melanesia (Palek and Lambert, 1990). Unlike other forms of HE, SAO is not associated with an increase in the percentage of SpD in the RBC membrane skeleton.

The molecular lesion responsible for SAO has been identified as a deletion of nine amino acids at the interface between the N-terminal cytoplasmic domain and the first transmembrane region in the anion transporter, band 3 (Jarolim et al., 1991; Schofield et al., 1992b). The rotational mobility of SAO band 3 is markedly reduced (Tilley et al., 1991), and it has been suggested that the reduction of mobility arises from the formation of microaggregates of SAO band 3 (Fig. 3 *c*).

The membranes of SAO RBCs are abnormally rigid, and micropipette aspiration yields a value for μ_m that is three to five times higher than that of normal RBC membranes (Tilley et al., 1991; Schofield et al., 1992b; Mohandas et al., 1992). Despite the significant increase in RBC membrane rigidity, SAO does not present any hematological complications. Interestingly, the SAO mutation of band 3 serves to protect affected individuals from the invasion of malaria parasites (Schofield et al., 1992b), but it is not known

whether this protection is derived from the increased membrane stiffness, or from metabolic differences of SAO RBCs.

The topology of the skeleton has not been characterized directly for SAO RBCs. However, EM images of freeze-fracture replicas of SAO RBCs reveal an irregular surface, with clusters of intramembrane particles (IMPs) aligned in single rows (Che et al., 1993; Liu et al., 1995). The IMPs contain band 3, and are approximately 11 nm in diameter, the same size as a dimer of band 3 subunits (Paulitschke et al., 1995; Liu et al., 1995). These IMPs form aggregates containing an average of eight IMPs, with a range of four to 21 IMPs per row (Liu et al., 1995). Normal RBC membranes exhibit the same number of IMPs, but without any cluster or row formation. It has been proposed that the three- to fivefold increase in μ_m of SAO RBCs may be a consequence of these chainlike aggregates of mutant band 3 restricting the relative motion of adjacent spectrin oligomers in the skeleton (Liu et al., 1995).

METHODS

Construction of networks

In previous work (Hansen et al., 1996), we described methods for constructing random networks, specifying the properties of elements that represent spectrin, and computing the elastic moduli of these networks by FEM analysis. Here we introduce variations in network topology to mimic the structure of normal and abnormal RBC skeletons. If it is assumed that the skeleton contains only tetramers ($\phi_s = 2$) and that an average of six tetramers are joined to each actin junction ($\phi_a = 6$), then the topology of the RBC membrane skeleton can be modeled by the positions of edges in a Delaunay triangulation, as described by Hansen et al. (1996). Here we use triangular networks that are essentially isotropic, with the normalized standard deviation of edge length (σ_L) in the range of $0.21 < \sigma_L < 0.23$.

Variations of ϕ_a and ϕ_s

To construct networks with a range of topologies, we begin with a Delaunay triangulation and perform a series of modifications. In a Delaunay triangular network, it is assumed that each edge represents one SpT and each vertex corresponds to an actin junction (Fig. 4 *a*). The number of spectrin dimers per self-association junction is thus $\phi_s = 2$, and there are an average of six edges per vertex, so $\phi_a = 6$. If some of the SpT's are removed from this network, we obtain values of $\phi_a < 6$, with $\phi_s = 2$ (Fig. 4 *b*).

Skeletons that contain SpH are modeled by creating networks with Y-shaped triads of spring elements. Starting with a Delaunay triangulation, each triangle in the network is considered as a possible site where an SpH may be inserted. For each SpH, three new edges (representing spectrin dimers) are created, with each binding to one of the vertices of the original triangle. A new node is inserted, equidistant from the vertices, and is considered to be the self-association site of the hexamer. This method for assigning positions of SpH ensures that all of the elements in the model network only meet in actin junctions or spectrin self-association sites. This is consistent with EM images of spread skeletons (Liu et al., 1987; Shen et al., 1986). If one SpH is inserted within each triangular region of a Delaunay triangulation, the resulting network has topological parameters $\phi_a = 6$ and $\phi_s = 3$ (Fig. 4 *c*). Then, by removal of some fraction of the SpH, the value of ϕ_a can be reduced, yielding topologies of $\phi_a < 6$, with $\phi_s = 3$ (Fig. 4 *d*). Intermediate values of ϕ_a and ϕ_s can be obtained by using various fractions of SpT and SpH (see Appendix).

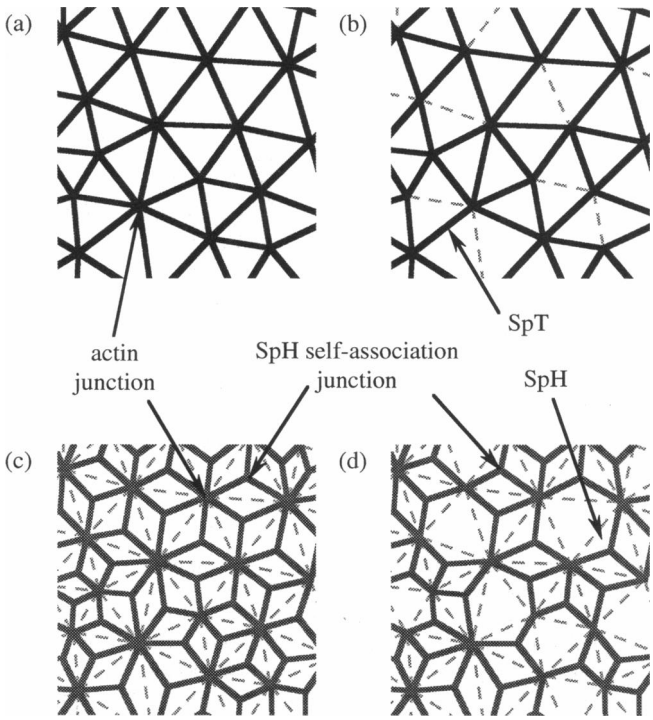

FIGURE 4 Constructing networks with a range of topologies. (*a*) Original triangular network, corresponding to the topological parameters $\phi_a = 6$, $\phi_s = 2$. Each edge represents one SpT. (*b*) Triangular network modified by removal of some SpT, so that $\phi_a < 6$, $\phi_s = 2$. (*c*) Network modified by removal of all SpT and insertion of one SpH within each triangular region of the original network. $\phi_a = 6$, $\phi_s = 3$. (*d*) Network modified by removal of some of the SpH in *c*, resulting in $\phi_a < 6$, $\phi_s = 3$. Vacant SpT sites are indicated by dashed lines.

Topology of the normal RBC membrane skeleton

Values of $\phi_a = 6.0$ and $\phi_s = 2.0$ are obtained with Delaunay triangular networks, which we denote by topology A, as shown in Fig. 5 *a*. An alternative topology B, with $\phi_a = 5.0$ and $\phi_s = 2.1$, is based on EM images of spread, negatively stained skeletons (Fig. 5 *b*). Topology C (Fig. 5 *c*), with $\phi_a = 4.2$ and $\phi_s = 2.3$, is based on EM images of skeletons prepared by the QFDERR technique. These networks serve as representations of normal skeletal topologies, as visualized by different techniques.

Modeling sparse networks

For the range of normal and pathological topologies we wish to consider, many of the networks are sparse and contain regions that can pivot and exhibit little or no resistance to shear deformation. This can result in numerical problems for the FEM solver. To circumvent this problem when SpT's are to be removed from the original triangular network (as indicated by the *dashed lines* in Fig. 4), the elements that should be removed are instead assigned a very small spring constant of $K' \ll K$ rather than exactly zero.

Abnormal skeletons: cross-linking

In some pathologies of the RBC membrane skeleton, the connectivity of the spectrin network may be increased due to additional intracellular or extracellular linkages. This type of skeletal modification is modeled by introducing cross-linking elements. We assume that cross-links only occur between the self-association sites of neighboring spectrin oligomers. This

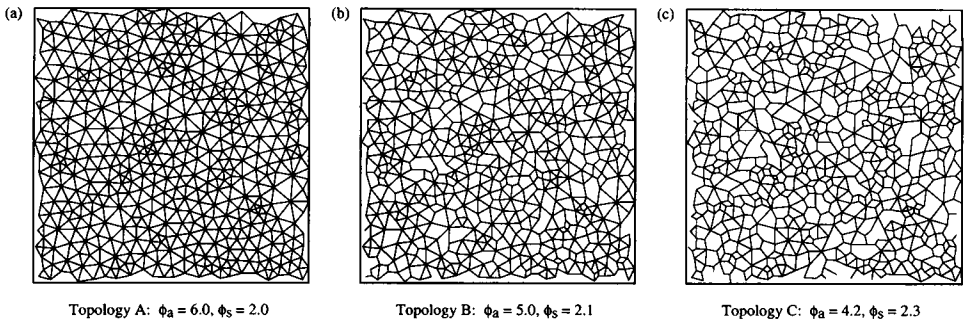

FIGURE 5 Examples of random networks used to model the topology of the normal RBC membrane skeleton. (*a*) Topology A: $\phi_a = 6.0$, $\phi_s = 2.0$, an approximation of skeletal topology that has been assumed in previous models. (*b*) Topology B: $\phi_a = 5.0$, $\phi_s = 2.1$, based on EM images of spread, negatively stained skeletons. (*c*) Topology C: $\phi_a = 4.2$, $\phi_s = 2.3$, based on EM images of skeletons prepared by the QFDERR technique. For the networks shown in *b* and *c*, the positions of SpT are dependent upon the positions of SpH (see text).

choice is made on the basis of evidence that mutant band 3 forms microaggregates in the membranes of SAO RBCs, and because ankyrin/band 3 junctions are bound to the skeleton near the self-association site of spectrin. To simplify the geometry of cross-linked networks, we assume that the ankyrin/band 3 junctions are coincident with the spectrin self-association sites, and neglect any differences between intracellular and extracellular cross-linking that might arise because of three-dimensional effects.

When a normal skeleton is modeled by topology A (Fig. 5 *a*), we assume that the midpoint of each edge corresponds to a SpT self-association site, and that cross-links may be inserted in groups of three, as shown in Fig. 6 *a*. The use of groups of three cross-links avoids the creation of unstable subgroups. When a particular SpT site is vacant, and the corresponding neighboring triangle contains an SpH, then the self-association site of that SpH may be used as a cross-linking site, as shown in Fig. 6 *b*.

Properties of the spectrin elements

The physical properties of spectrin are represented in the model by the force-extension relation of each of the elastic spring elements. Here we assume that spectrin obeys a linear force-extension relation ($F = K\Delta L$), that spectrin forms freely rotating connections at actin junctions, and that each spring is stress-free in the initial configuration of the network (see Hansen et al., 1996). Because elements in random networks necessarily have different lengths, the spring constant of the *i*th element is defined as a function of its initial length, L_i: $K_i = K\bar{L}/L_i$, where K is a reference value that corresponds to a spring of length $\bar{L}$, the mean element length.

Very compliant springs (that represent missing elements) and cross-linking springs are assigned values for spring constants in terms of K, the reference value for the spring constant of a tetramer. As shown in Fig. 10, weak cross-linking springs ($K_{XL} < K$) have a negligible effect on network elasticity.

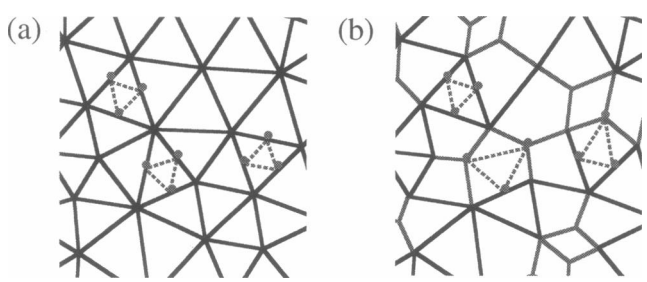

FIGURE 6 Simulation of cross-links. (*a*) When topology A is used to model a normal skeleton, sets of cross-links are introduced between the self-association sites of adjacent SpT. (*b*) When a normal skeleton is modeled by topology B or C, cross-links may also be attached to the self-association sites of SpH. Cross-links are represented by dashed lines.

Computation of elastic moduli

Networks are subjected to prescribed boundary node displacements that correspond to a homogeneous deformation with the principal extension ratios λ_1 and λ_2. The deformed positions of all internal nodes are then computed by the commercial finite-element program ABAQUS (Hibbitt, Karlsson, and Sorensen, Rhode Island). The strain energy density (Ψ) of a deformed network is computed as the sum of the energies of all elements, divided by the area of the network in its reference configuration. Then Ψ is used to compute the elastic moduli of the corresponding equivalent continuum, assuming an isotropic, homogeneous elastic material undergoing finite deformations (Evans and Skalak, 1980). This formulation is based on two deformation parameters: the fractional area expansion, $\alpha = \lambda_1\lambda_2 - 1$; and the degree of shear, $\beta = [(\lambda_1 + \lambda_2)/(2\lambda_1\lambda_2)] - 1$. The shear modulus is defined as $\mu = \partial\psi/\partial\beta$, for constant α, and the area expansion modulus is defined as $\kappa = \partial^2\psi/\partial\alpha^2$, for constant β. Both μ and κ are functions of α and β. For small strains, μ and κ correspond to the usual two-dimensional definitions of shear and areal moduli (Hansen et al., 1996).

RESULTS

Variation of μ and κ with ϕ_a and ϕ_s

For model networks with a range of topologies, μ and κ are computed for the case of small deformations (i.e., $\mu = \partial\psi/\partial\beta$ and $\kappa = \partial^2\psi/\partial\alpha^2$, evaluated at $\alpha = 0$ and $\beta = 0$). Because μ and κ scale directly with the linear spring constant (K), the elastic moduli are reported as the normalized quantities μ/K and κ/K.

In Fig. 7 *a*, μ/K is shown as a function of ϕ_a, for several values of ϕ_s. Symbols indicate results of FEM computations for 480 different networks, and the solid lines represent least-squares approximations for each set of data. Networks that are characterized by similar topological parameters (ϕ_a, ϕ_s) may have different mechanical properties, as indicated by the degree of scatter in Fig. 7 *a*. Computed values for κ/K are processed in a similar manner, as shown in Fig. 7 *b*.

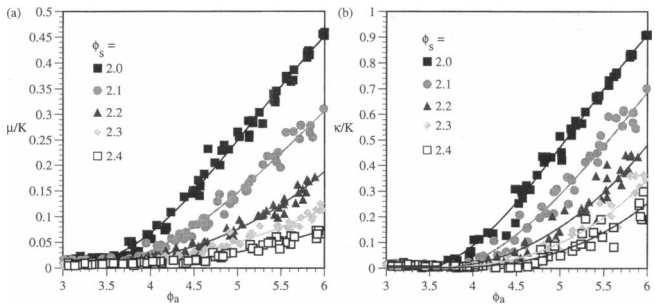

FIGURE 7 (*a*) Normalized shear modulus μ/K versus ϕ_a, for several values of ϕ_s. (*b*) Normalized area expansion modulus κ/K versus ϕ_a, for several values of ϕ_s. Symbols indicate the results of FEM computations for several different networks, and the solid lines represent approximations for each value of ϕ_s.

Modeling the topology of the normal RBC membrane skeleton

Three particular topologies, which we denote by A, B, and C, are studied in detail. These topologies correspond to the various proposed models for the normal RBC membrane skeleton, as shown by the sample networks in Fig. 5, *a–c*. Topology A, characterized by $\phi_a = 6$ and $\phi_s = 2$, has been assumed in several previous mechanical models of the RBC membrane skeleton (Stokke et al., 1986; Kozlov and Markin, 1987; Boal, 1994). For the degree of randomness chosen for this analysis ($\sigma_L = 0.20$), the normalized elastic moduli have values of $\mu/K = 0.455 \pm 0.003$ and $\kappa/K = 0.908 \pm 0.002$ in small deformations (mean $\pm$ standard deviation, $n = 5$). Other choices of σ_L yield similar results.

Topology B (Fig. 5 *b*), characterized by $\phi_a = 5.0$, $\phi_s = 2.1$, is based on EM images of spread, negatively stained skeletons. For model networks with topologies in the range of $4.95 < \phi_a < 5.05$ and $2.09 < \phi_s < 2.11$, the model predicts $\mu/K = 0.172 \pm 0.013$ and $\kappa/K = 0.587 \pm 0.056$ (mean $\pm$ SD, $n = 12$).

Topology C (Fig. 5 *c*), with $\phi_a = 4.2$, $\phi_s = 2.3$, is based on EM images of skeletons prepared by the QFDERR technique. For model networks with topologies in the range of $4.15 < \phi_a < 4.25$ and $2.28 < \phi_s < 2.32$, we obtain values of $\mu/K = 0.0174 \pm 0.0042$ and $\kappa/K = 0.235 \pm 0.056$ ($n = 13$). These results are summarized in Table 3.

The networks subjected to these computations contain some very compliant springs, with $K'/K = 10^{-6}$, to represent "vacant" SpT sites. To show that the results are not influenced by the use of such very compliant springs, we computed μ/K as a function of K'/K for topologies B and C, as plotted in Fig. 8, which shows that very compliant springs do not affect results when $K'/K \leq 10^{-3}$.

Variation of μ in large deformations

Networks corresponding to topologies A and B were subjected to large deformations, to compute the dependence of μ/K on α and β. The results are shown in Fig. 9 as ratios μ/μ_o, where μ_o is the shear modulus for small deformations

TABLE 3 Computed values of the normalized shear modulus, μ/K, and the normalized area expansion modulus, κ/K, for three topological models of the normal RBC membrane skeleton

	A	B	C
ϕ_a	6.0	5.0	4.2
ϕ_s	2.0	2.1	2.3
μ/K	0.455 ± 0.003	0.172 ± 0.013	0.0174 ± 0.0042
κ/K	0.908 ± 0.002	0.587 ± 0.056	0.235 ± 0.056
K (dyn/cm)	0.017 ± 0.004	0.045 ± 0.013	0.48 ± 0.20

For each topology, the effective stiffness of spectrin (K) is computed by assuming $\mu = \mu_m$, where the value of the RBC membrane shear modulus measured by micropipette aspiration is assumed to be $\mu_m = 7.5 \times 10^{-3}$ dyn/cm.

(i.e., at $\alpha = 0$, $\beta = 0$). The relative shear modulus, μ/μ_o, depends on α, β, and network topology, but is independent of the value of K. μ/μ_o increases with both the degree of shear and the degree of isotropic expansion. For shear deformations characterized by large values of β, some elements in a network will begin to exhibit "cross-over," meaning that these springs overlap at locations other than their end points. This occurs because the spring elements in the model are not self-avoiding. Because this is not expected to happen in the RBC membrane skeleton, we limit our analysis to deformations that do not induce cross-over. This accounts for the limited range of β spanned by results for topology B in Fig. 9 *b*. For networks representing topology C, μ increases with β in a similar manner.

Variation of μ with degree of cross-linking

The degree of cross-linking is quantified as the ratio XL/N_d, where XL is the number of cross-linking springs inserted in the network and N_d is the number of spectrin dimers in the network. For topology A (Fig. 5 *a*), the maximum value of

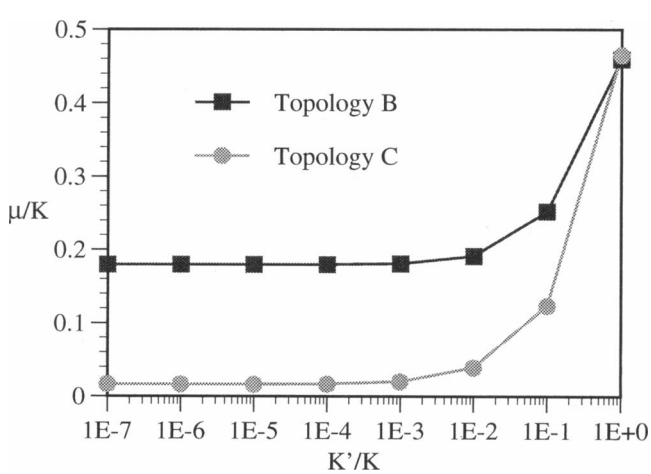

FIGURE 8 Variation of μ/K with the stiffness of the very compliant springs (K'/K) representing missing elements in a network. For networks corresponding to topologies B or C, the use of very compliant springs with $K'/K \leq 10^{-3}$ eliminates numerical problems with the FEM solver, but does not alter the results.

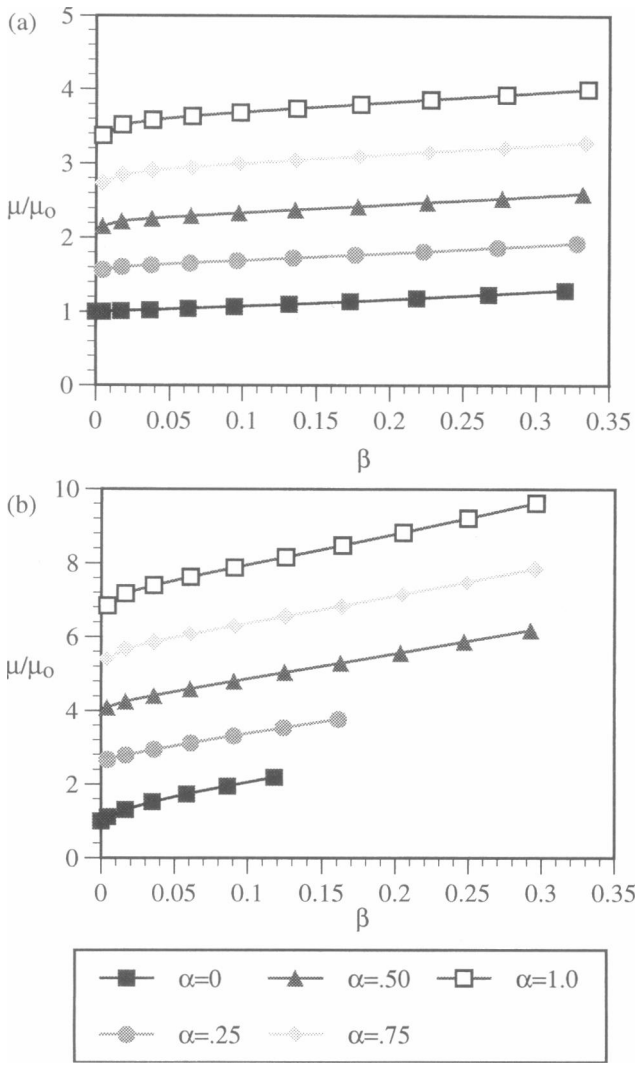

FIGURE 9 Variation of the relative shear modulus (μ/μ_o) in large deformations, computed for model networks with topology A (*a*) or topology B (*b*), where μ_o is the shear modulus of the same network in small deformations ($\alpha = 0$, $\beta = 0$).

XL/N_d is approximately 1, because each triangle in the network can contain three cross-links. In topologies B and C, the maximum degrees of cross-linking are ~0.80 and ~0.60.

For a network with a particular degree of cross-linking, the computed value of μ/K varies, of course, with the stiffness of the cross-linking springs, K_{XL}/K. Fig. 10 illustrates this phenomenon for a network with topology A and $XL/N_d = 0.5$ (about one-half of the triangles in the network contain sets of cross-links). In this case, μ_o is the shear modulus of the same network without cross-linking. The relative shear modulus approaches a maximum value when $K_{XL}/K \approx 500$, and is unchanged for larger values of K_{XL}/K. The cross-links with $K_{XL}/K \geq 500$ behave as essentially rigid elements.

Using cross-links with $K_{XL}/K = 1000$, we next computed μ/K for a range of values of XL/N_d. As shown in Fig. 11, μ/K increases with XL/N_d for all three models of skeletal topology. It is readily seen that topology A is least affected by cross-linking (Fig. 11 *b*).

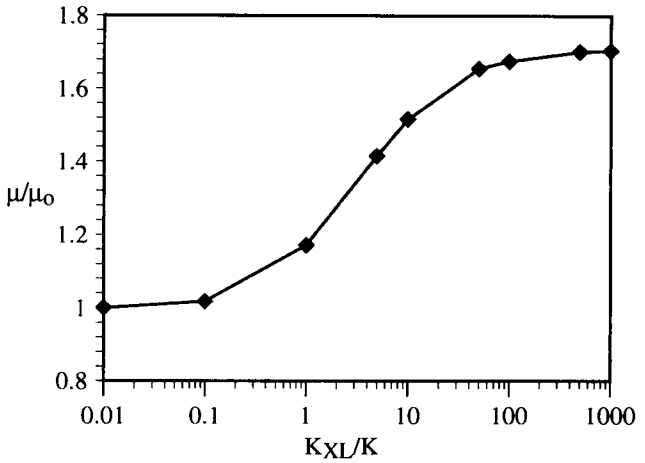

FIGURE 10 Variation in the relative shear modulus, μ/μ_o, with the stiffness of cross-linking springs, K_{XL}/K, for model network topology A. The shear modulus (μ) is computed for a cross-linked network with $XL/N_d = 0.5$, and μ_o is the shear modulus of the same network without cross-linking ($XL = 0$). Note that weak cross-linking springs have a negligible effect on network elasticity, and the maximum value of μ/μ_o is unchanged for $K_{XL}/K \geq 500$, indicating that such springs behave as essentially rigid elements.

DISCUSSION

Elasticity of the normal RBC membrane skeleton

Our results demonstrate that variations in topology have significant effects on the macroscopic elastic properties of a model network. Among the three models considered for normal skeletons, we find that the computed values of μ/K vary by more than an order of magnitude. To determine what value of K is needed to create a model that mimics the macroscopic behavior of the RBC membrane, we assume that the shear modulus of the intact RBC membrane (μ_m), as measured by micropipette aspiration, is equal to the shear modulus (μ) computed by the model, so $\mu \approx \mu_m$. Experimental values for μ_m vary from 6×10^{-3} to 9×10^{-3} dyn/cm, with an average value of $\mu_m = 7.5 \times 10^{-3}$ dyn/cm (Chien et al., 1978; Waugh and Evans, 1979; Hochmuth and Waugh, 1987). Then for each topology (and each value of μ/K) we obtain the corresponding value for K.

As shown in Table 3, topology A (Fig. 5 *a*) has the highest value of μ/K and consequently yields the lowest value for the effective K of spectrin. Note that μ/K decreases significantly for the relatively sparse topologies B and C, so that the individual springs in these networks must be much stiffer to produce the same degree of macroscopic shear elasticity given by μ_m. In Fig. 12, the relationship between K and μ/K is shown as a solid line, with three bars indicating the results for topologies A, B, and C, and the assumed relations $\mu_m \approx \mu$ and $\mu_m \approx \mu\kappa/(\mu + \kappa)$.

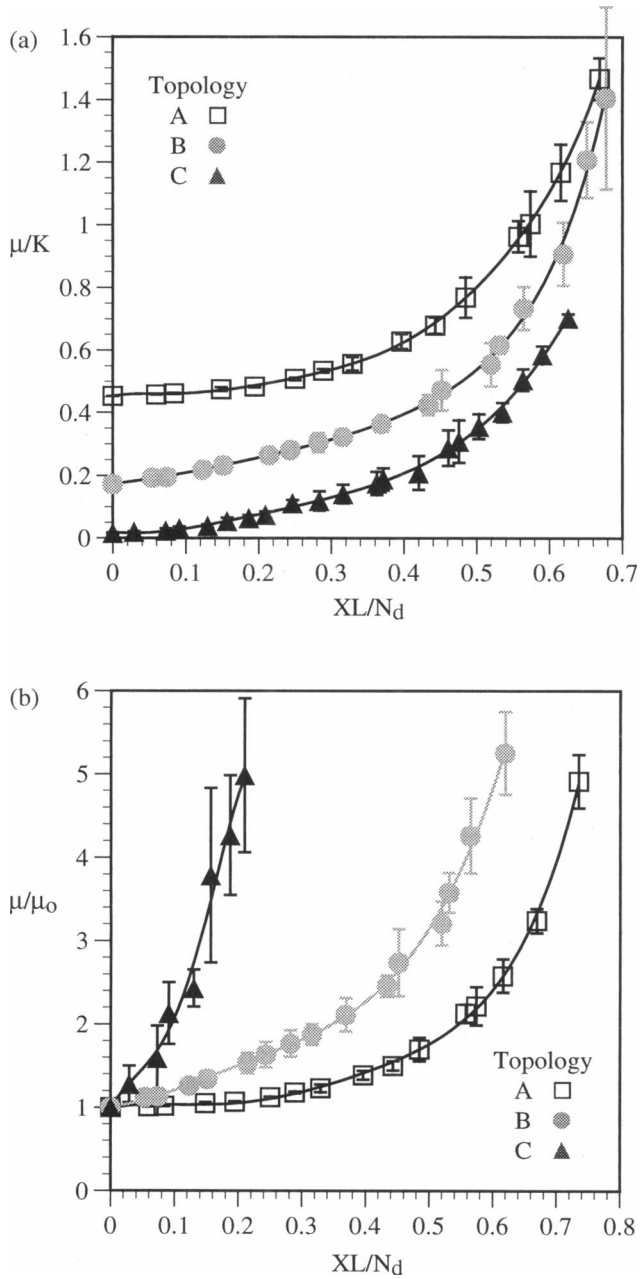

FIGURE 11 Increase in the computed shear modulus of model networks due to the introduction of rigid cross-links (K_{XL}/K = 1000), for three different initial topologies. (*a*) Normalized shear modulus, μ/K, versus the degree of cross-linking, XL/N_d. (*b*) Relative shear modulus, μ/μ_o, versus XL/N_d. Each point represents the mean values of μ/K (or μ/μ_o) and XL/N_d for five networks with similar topologies (ϕ_a, ϕ_s) and similar degrees of cross-linking.

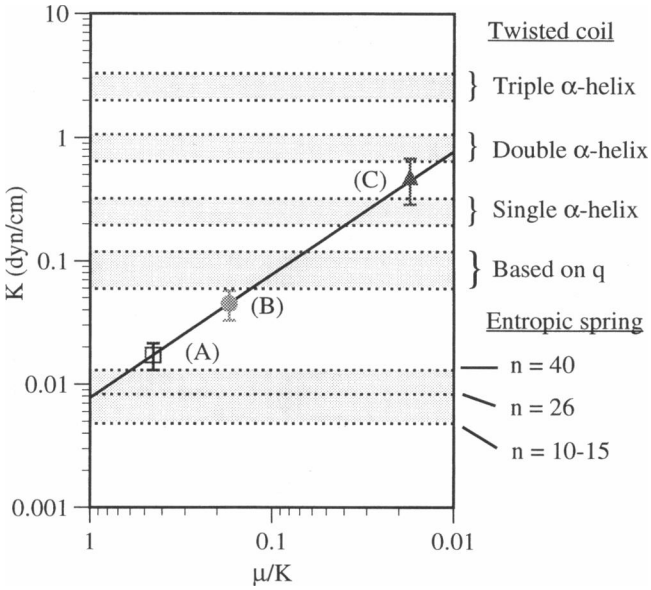

FIGURE 12 Comparison of K derived from μ/K and μ_m with K predicted by various models for spectrin extension, FEM simulations, and micropipette measurements of the RBC membrane. Results for three particular topological models are shown: (*A*) ϕ_a = 6.0 and ϕ_s = 2.0, with μ/K = 0.45; (*B*) ϕ_a = 5.0 and ϕ_s = 2.1, with μ/K = 0.172; (*C*) ϕ_a = 4.2 and ϕ_s = 2.3, with μ/K = 0.017. The shaded bands represent estimates based on various spectrin models (see text). The stiffness of an entropic spring varies with the number of links (n) in a long-chain molecule. The extensional stiffness of a twisted coil varies with the bending stiffness of each of the subunits of spectrin, as estimated from the measured persistence length (q) of spectrin, or theoretical predictions for the stiffness of a single α-helix, double α-helical coil, or triple α-helical coil.

In Hansen et al. (manuscript submitted for publication), ranges of likely values for K were computed on the basis of an entropic spring model and a twisted coil model for spectrin elasticity. These ranges are shown as shaded regions in Fig. 12. The stiffness of an entropic spring varies with the number of links (n) in a long-chain molecule. The extensional stiffness of a twisted coil varies with the bending stiffness of each of the subunits of spectrin, as estimated from the measured persistence length (q) of spectrin, or theoretical predictions for the stiffness of a single α-helix, double α-helical coil, or triple α-helical coil. We expect that the elasticity of spectrin is better represented by the twisted-coil model, because recent structural data indicate that spectrin is a staggered triple-coiled coil, and does not possess flexible hinges, as assumed for the entropic spring model. As shown in Fig. 12, data for topology C, which most closely resemble the normal skeleton, support the twisted-coil model of spectrin elasticity.

Hereditary spherocytosis

To model the reduction in spectrin content associated with HS, we begin with a particular normal network topology, and reduce ϕ_a by reducing N_d, i.e., by removing elements. In Fig. 13 we compare the model results to measured properties of spectrin-deficient RBCs in HS (Waugh, 1987; Waugh and Agre, 1988). The reduction in μ/K with decreased ϕ_a varies with the choice of topology A, B, or C for a normal skeleton (Fig. 13 *a*). Computed values of μ/μ_o are plotted as functions of N_d/N_{do} in Fig. 13 *b*, where μ_o corresponds to the elasticity of a network with initial topology A, B, or C; N_{do} is the number of spectrin dimers in the

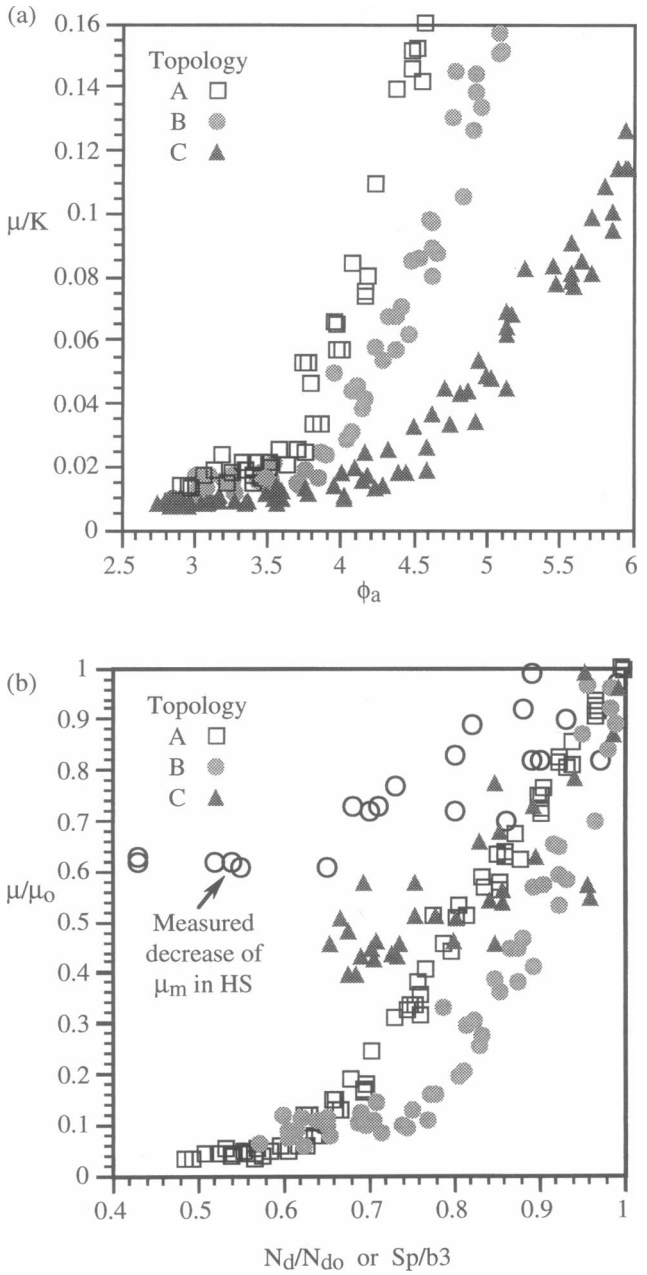

FIGURE 13 Decrease in the computed shear modulus due to the removal of spectrin elements from model networks, for three different initial topologies. (*a*) Normalized shear modulus, μ/K, versus the average number of spectrin oligomers per actin junction, ϕ_a. (*b*) Relative shear modulus, μ/μ_o, versus the reduction in the number of spectrin dimers in the network, N_d/N_{do}, or equivalently, the ratio of spectrin to band 3 measured by gel densitometry, Sp/b3 (see text). The measured reduction in shear modulus for HS RBCs is shown by open circles in *b*, as reported by Waugh and Agre (1988).

initial network; and N_d is the number of dimers in the depleted network. The ratio N_d/N_{do} is equivalent to the experimental measurement of Sp/b3, the mass of spectrin normalized relative to the mass of band 3 in the membrane. For HS RBCs with Sp/b3 in the range of 40–70%, the experimental data suggest that μ_m decreases in proportion to the degree of spectrin deficiency. For Sp/b3 below 70%, the measured value of μ_m does not fall below ~60% of the normal membrane elasticity (Fig. 13 *b*, *open circles*). This trend in the experimental data is approximately reproduced by our results for model networks with initial topologies A, B, or C. However, for initial topologies A and B, μ/μ_o approaches a relatively low value of ~0.05–0.10. For initial topology C, the same degree of spectrin deficiency results in a much higher value of $\mu/\mu_o \approx 0.50$, so networks representing topology C appear to be most consistent with the HS RBC data.

Southeast Asian ovalocytosis

The topological alterations associated with SAO are modeled by introducing cross-linking elements that correspond to chains of IMPs. The IMPs are primarily composed of band 3, a globular protein that is expected to be much less deformable than spectrin. Therefore, in a model network chains of IMPs are represented by cross-linking springs that are essentially rigid relative to the springs that correspond to spectrin ($K_{XL}/K = 1000$).

To quantify the degree of cross-linking in the SAO skeleton, we estimate that each RBC contains 2×10^5 SpD and 6×10^5 band 3 dimers (Paulitschke et al., 1995). In an SAO RBC, 40% of the band 3 is abnormal, and 25% of this mutant band 3 is extracted from the skeleton in dimeric form, presumably corresponding to the fraction that is not bound to the skeleton (Liu et al., 1995). Therefore, approximately 1.8×10^5 mutant band 3 dimers, or equivalently 1.8×10^5 IMPs, are expected to participate in aggregate formation and serve as cross-links for the underlying skeleton. To effectively join two adjacent spectrin self-association sites in the underlying skeleton, a row of IMPs must span ~35 nm, assuming that the length of one SpT in the undeformed skeleton is 70 nm. That a single IMP has a diameter of 11 nm (Paulitschke et al., 1995; Liu et al., 1995) indicates a ratio of about three IMPs per cross-link (*XL*) in the model. Therefore a typical SAO RBC is expected to contain ~0.3 XL/N_d, where *XL* is the number of cross-links between adjacent spectrin oligomers, and N_d is the number of spectrin dimers in the skeleton.

Recall that SAO RBCs exhibit a three- to fivefold increase in μ_m. In our computations, this corresponds to $3 < \mu/\mu_o < 5$, as shown by the dashed box in Fig. 14. The effects of cross-linking vary considerably with the choice of topology for a normal skeleton. For example, μ/μ_o in the range of 3 to 5 is induced by $XL/N_d = 0.66–0.75$, 0.48–0.60, and 0.15–0.21, for initial topologies A, B, and C, respectively. The behavior of SAO RBCs is intermediate to that of model networks with topologies B and C, although a closer agreement is obtained with topology C.

Other skeletal defects

A number of other defects also result in structural and mechanical abnormalities of the RBC membrane skeleton,

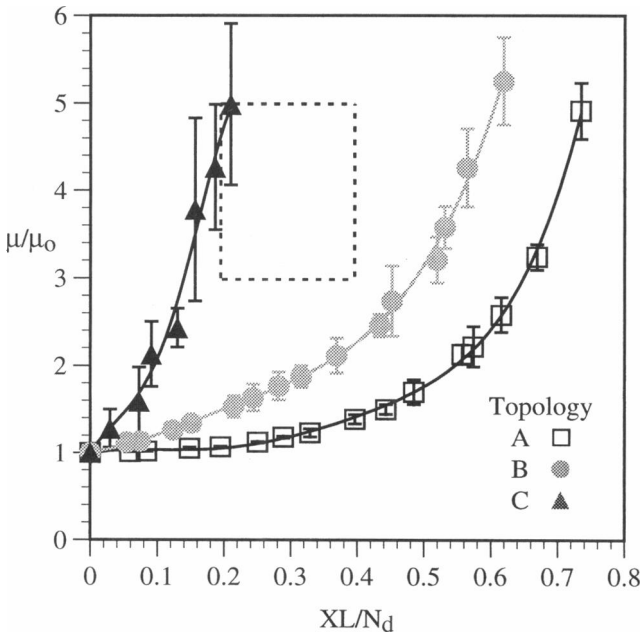

FIGURE 14 Comparison of computed values of μ/μ_o for cross-linked model networks with the properties of SAO skeletons. With $XL/N_d \approx 0.3$, SAO RBCs exhibit a three- to fivefold increase in the membrane shear modulus (*region enclosed by dashed box*). This behavior falls between the computed properties of networks with topologies B and C.

but the molecular-level consequences of most defects are not well characterized, and the currently available information is not sufficient to establish the mechanisms by which mechanical changes may be induced. In these cases, our model may be helpful for investigating structure-function relationships in abnormal RBCs if measurements of μ_m are available and if the structural defect has been partially characterized. Here we discuss one such case: hereditary elliptocytosis (HE).

In certain forms of HE, the major defect produces an increase in unassociated spectrin dimers (SpD's) (Palek and Jarolim, 1993; Palek, 1985). These defects typically disrupt an α-helical region in spectrin and cause unwinding of the α and β subunits (Sahr et al., 1993). However, HE RBCs exhibit an increase in μ_m that cannot be explained by the increase in unassociated SpD's. For an unassociated dimer mass fraction in the range of 0.15–0.25, μ_m is increased by a factor of 1.5–2.5 (Chabanel et al., 1989). This mechanical behavior differs strikingly from the decreased μ_m of HS RBCs, indicating that skeletons with broken spectrin links (HE) cannot be accurately represented by the same types of models that apply to skeletons with missing links (HS). This suggests that current knowledge of the structure of HE RBCs is probably too incomplete to develop a reliable model. Hence in the present paper HE is not explicitly modeled, although our methods can be used to investigate a variety of possible structural changes and suggest which of these might induce an increase in μ that is consistent with μ_m of HE RBCs. Then our methods may be helpful for formulating hypotheses and for directing future experimental work.

For example, an increase in macroscopic membrane stiffness may be explained by the presence of cross-links, as shown by our results for SAO. It is possible that the unwound spectrin subunits in unassociated SpD's may participate in cross-linking interactions with adjacent unwound subunits, or with other components of the skeleton. (Unassociated spectrin is known to form aggregates with hemoglobin (Kiefer et al., 1995).) Although HE RBCs exhibit abnormalities in skeletal topology (Coetzer et al., 1990; Liu et al., 1990a; Ohno et al., 1993; Maréchal et al., 1994), such cross-links have not been reported.

In addition to the genetic defects discussed here (HS, SAO, HE), the structure of the RBC membrane skeleton is altered as a secondary consequence of various other diseases, such as sickle cell disease (Liu et al., 1991; Mackie and Hochmuth, 1990), β-thalassemia (Scott et al., 1990), and diabetes (Schwartz et al., 1991). Topological changes may also be associated with RBC aging, and the mechanisms by which senescent RBCs are recognized and removed from the circulation. Many physiochemical treatments are also known that alter skeletal structure and RBC membrane stiffness, including exposure to cross-linking agents (Fischer et al., 1978; Chabanel et al., 1989; Paulitschke et al., 1995) and the thermal denaturation of spectrin (Rakow and Hochmuth, 1975). As described for the case of HE, this network model can be used to test a variety of hypotheses for the mechanisms by which membrane elasticity is altered.

Extensions of this network model

This modeling approach is highly versatile and can be improved by incorporating new information as it becomes available. Additional research is still needed regarding the structural organization of the skeleton in its native state, for normal as well as abnormal RBCs. Atomic force microscopy has already been used to resolve molecular-level details of biological membranes under physiological conditions (Häberle et al., 1991; Miyamoto et al., 1993; Mikrut and MacDonald, 1994) and offers promise for more detailed studies of RBC skeletal topology in intact cells and membrane samples.

In the future, network models may be used to address additional questions regarding the relationship between skeletal topology, spectrin properties, and membrane elasticity in normal and abnormal RBCs. It has recently been proposed that the RBC membrane skeleton may be a dynamic structure that regulates its elasticity in response to varying concentrations of endogenous metabolic agents (Brody et al., 1995; Manno et al., 1995). Our methods may be adapted to study the possible effects of dynamic structural changes by introducing appropriate rate constants for topological changes. A further step in dynamic modeling may involve modifications of the network as a function of time and deformation that lead to macroscopic plasticity.

APPENDIX

Construction of a network with specified topological parameters ϕ_a and ϕ_s

To produce a network with a specified topology (ϕ_a, ϕ_s), a Delaunay triangular network is first constructed (see Hansen et al., 1996). All enclosed regions within the network are then triangles and all edges are considered to be spring elements representing spectrin tetramers (SpT's). Furthermore, each triangular region defines a potential site where a hexamer (SpH) may be inserted in the network (Fig. 4 *c*). Modified networks are created by removing some of the tetramers and adding hexamers to some of the potential SpH sites. In the final network, the fraction of tetramer sites that are still occupied is defined as f_{tet}, and the fraction of potential hexamer sites that are occupied is defined as f_{hex}. The fraction of the original actin junctions that are still connected to the rest of the network by at least two spectrin elements in the final network is denoted by f_{act}. The values of f_{tet} and f_{hex} may vary between 0 and 1.0, whereas f_{act} will typically be close to 1.0, unless a large proportion of the original edges are removed, in which case f_{act} approaches 2/3. Other topological parameters of the final network include the number of tetramers (N_t), the number of hexamers (N_h), the number of spectrin dimers in the network (N_d), the number of spectrin self-association sites (N_s), and the number of actin junctions in the network (N_a).

Recall that the number of points (N_P), edges (N_E), and cells (N_C) in a Delaunay triangulation are related by $N_E = 3N_P$ and $N_C = 2N_P$, provided that the effects of network boundaries are neglected (Okabe et al., 1992). Then the following relations are valid for a modified network that is obtained from a Delaunay network with P points:

$$N_t = 3N_P f_{tet}, \quad N_h = 2N_P f_{hex},$$
$$N_d = 2N_t + 3N_h = 6N_P f_{tet} + 6N_P f_{hex}, \qquad \text{(A1)}$$
$$N_s = N_t + N_h = 3N_P f_{tet} + 2N_P f_{hex}, \quad \text{and} \quad N_a = N_P f_{act}.$$

Expressions for ϕ_a and ϕ_s may be derived as functions of the fractions of SpT and SpH sites filled. Note that the average functionality of actin junctions is equivalent to the number of dimers in the network divided by the number of actin junctions:

$$\phi_a = \frac{N_d}{N_a} = \frac{6Pf_{tet} + 6Pf_{hex}}{Pf_{act}} = \frac{6(f_{tet} + f_{hex})}{f_{act}}. \qquad \text{(A2)}$$

The average functionality of spectrin self-association sites is determined in a similar manner:

$$\phi_s = \frac{N_d}{N_s} = \frac{6Pf_{tet} + 6Pf_{hex}}{3Pf_{tet} + 2Pf_{hex}} = \frac{6(f_{tet} + f_{hex})}{(3f_{tet} + 2f_{hex})}. \qquad \text{(A3)}$$

Equations A2 and A3 can be solved for f_{tet} and f_{hex}:

$$f_{tet} = \phi_a f_{act}\left(\frac{3 - \phi_s}{3\phi_s}\right), \quad f_{hex} = \phi_a f_{act}\left(\frac{\phi_s - 2}{2\phi_s}\right). \qquad \text{(A4)}$$

Given the desired topological parameters ϕ_a and ϕ_s that describe a particular topology we wish to imitate, we use Eq. A4 to compute f_{tet} and f_{hex}. Then a random number between 0 and 1 is generated for each potential spring location and compared to either f_{tet} or f_{hex}, depending on whether the location is a potential SpT site or SpH site. If the random number exceeds the corresponding fraction parameter, then that site is considered as vacant in the model, but if the random number is less than the fraction parameter, the site is occupied in the final network.

We gratefully acknowledge the helpful discussions with M. Ostoja-Starzewski, M. Dembo, and L. A. Sung.

This work was supported by a predoctoral fellowship from the American Heart Association, California Affiliate (JCH), a National Science Foundation predoctoral fellowship (JCH), an National Science Foundation PYI grant (CMS 90-57629 to AH), a grant from the Whitaker Foundation (AH), and National Institutes of Health grants HL-43026 (RS and SC) and HL-44147 (SC).

REFERENCES

Becker, P. S., and S. E. Lux. 1985. Hereditary spherocytosis and related disorders. *Clin. Haematol.* 14:15–43.

Bennett, V., and D. Gilligan. 1993. The spectrin-based membrane skeleton and micron-scale organization of the plasma membrane. *Annu. Rev. Cell Biol.* 9:27–66.

Boal, D. 1994. Computer simulation of a model network for the erythrocyte cytoskeleton. *Biophys. J.* 67:521–529.

Brody, J. P., Y. Han, R. H. Austin, and M. Bitensky. 1995. Deformation and flow of red blood cells in a synthetic lattice: evidence for an active skeleton. *Biophys. J.* 68:2224–2232.

Byers, T. J., and D. Branton. 1985. Visualization of the protein associations in the erythrocyte membrane skeleton. *Proc. Natl. Acad. Sci. USA.* 82:6153–6157.

Chabanel, A., K. L. P. Sung, J. Rapiejko, J. T. Prchal, S. C. Liu, and S. Chien. 1989. Viscoelastic properties of red cell membrane in hereditary elliptocytosis. *Blood.* 73:592–5.

Che, A., R. J. Cherry, L. H. Bannister, and A. R. Dluzewski. 1993. Aggregation of band 3 in hereditary ovalocytic red blood cell membranes: electron microscopy and protein rotational diffusion studies. *J. Cell Sci.* 105:655–660.

Chien, S., and L. Sung. 1990. Molecular basis of red cell membrane rheology. *Biorheology.* 27:327–344.

Chien, S., K. Sung, R. Skalak, S. Usami, and A. Tözeren. 1978. Theoretical and experimental studies on viscoelastic properties of erythrocyte membrane. *Biophys. J.* 24:463–487.

Coetzer, T., J. Palek, J. Lawler, S. Liu, P. Jarolim, M. Lahav, J. Prchal, W. Wang, B. Alter, G. Schweitz, V. Mankad, R. Gallanello, and A. Cao. 1990. Structural and functional heterogeneity of alpha spectrin mutations involving the spectrin heterodimer self-association site: relationships to hematologic expression of homozygous hereditary elliptocytosis and hereditary pyropoikilocytosis. *Blood.* 75:2235–2244.

Derick, L. H., S.-C. Liu, A. H. Chishti, and J. Palek. 1992. Protein immunolocalization in the spread erythrocyte membrane skeleton. *Eur. J. Cell. Biol.* 57:317–320.

Deuticke, B., R. Grebe, and C. W. M. Haest. 1990. Action of drugs on the erythrocyte membrane. *In* Blood Cell Biochemistry. Plenum Press, New York. 475–529.

Evans, E., and R. Skalak. 1980. Mechanics and Thermodynamics of Membranes. CRC Press, Boca Raton, FL.

Fischer, T. M., C. W. M. Haest, M. Stohr, D. Kamp, and B. Deuticke. 1978. Selective alteration of erythrocyte deformability by SH-reagents: evidence for an involvement of spectrin in membrane shear elasticity. *Biochim. Biophys. Acta.* 510:270–282.

Gilligan, D., and V. Bennett. 1993. The junctional complex of the membrane skeleton. *Semin. Hematol.* 30:74–83.

Häberle, W., J. Hörber, and G. Binnig. 1991. Force microscopy on living cells. *J. Vac. Sci. Technol.* B9:1210–1213.

Hansen, J. C., R. Skalak, S. Chien, and A. Hoger. 1996. An elastic network model based on the structure of the red blood cell membrane skeleton. *Biophys. J.* 70:146–166.

Hochmuth, R. M., and R. E. Waugh. 1987. Erythrocyte membrane elasticity and viscosity. *Annu. Rev. Physiol.* 49:209–219.

Jarolim, P., J. Palek, D. Amato, K. Hassan, P. Sapak, G. T. Nurse, H. L. Rubin, S. Zhai, K. E. Sahr, and S. C. Liu. 1991. Deletion in erythrocyte band 3 gene in malaria-resistant Southeast Asian ovalocytosis. *Proc. Natl. Acad. Sci. USA.* 88:11022–11026.

Kiefer, C. R., J. F. Trainor, J. B. McKenney, C. R. Valeri, and L. M. Snyder. 1995. Hemoglobin-spectrin complexes: interference with spectrin tetramer assembly as a mechanism for compartmentalization of band 1 and band 2 complexes. *Blood.* 86:366–371.

Kozlov, M. M., and V. S. Markin. 1987. Model of red blood cell membrane skeleton: electrical and mechanical properties. *J. Theor. Biol.* 129: 439–452.

Liu, S.-C., L. H. Derick, P. Agre, and J. Palek. 1990a. Alteration of the erythrocyte membrane skeletal ultrastructure in hereditary spherocytosis, hereditary elliptocytosis, and pyropoikilocytosis. *Blood.* 76: 198–205.

Liu, S., L. Derick, and J. Palek. 1987. Visualization of the hexagonal lattice in the erythrocyte membrane skeleton. *J. Cell Biol.* 104:527–536.

Liu, S.-C., L. H. Derick, and J. Palek. 1990b. Molecular anatomy of erythrocyte membrane skeleton in health and disease. *In* Cellular and Molecular Biology of Normal and Abnormal Erythroid Membranes. Wiley-Liss, New York. 171–183.

Liu, S.-C., L. Derick, S. Zhai, and J. Palek. 1991. Uncoupling of the spectrin-based skeleton from the lipid bilayer in sickled red cells. *Science.* 252:574–6.31.

Liu, S.-C., J. Palek, S. J. Yi, P. E. Nichols, L. H. Derick, S. Chiou, D. Amato, J. D. Corbett, M. R. Cho, and D. E. Golan. 1995. Molecular basis of altered red blood cell membrane properties in southeast Asian ovlaocytosis: role of the mutant band 3 protein in band 3 oligomerization and retention by the membrane skeleton. *Blood.* 86:349–358.

Liu, S., P. Windisch, S. Kim, and J. Palek. 1984. Oligomeric states of spectrin in normal erythrocyte membranes: biochemical and electron microscope studies. *Cell.* 37:587–594.

Mackie, L. H., and R. M. Hochmuth. 1990. The influence of oxygen tension, temperature, and hemoglobin concentration on the rheologic properties of sickle erythrocytes. *Blood.* 76:61256–61261.

Manno, S., Y. Takakuwa, K. Nagao, and N. Mohandas. 1995. Modulation of erythrocyte membrane mechanical function by spectrin phosphorylation and dephosphorylation. *J. Biol. Chem.* 270:5659–5665.

Maréchal, J., H. Wada, T. Koffa, A. Kanzaki, R. Wilmotte, K. Ikoma, A. Yawata, T. Inoue, K. Takanashi, A. Miura, N. Alloisio, J. Delaunay, and Y. Yawata. 1994. Hereditary elliptocytosis associated with spectrin Le Puy in a Japanese family: ultrastructural aspect of the red cell skeleton. *Eur. J. Haematol.* 52:92–98.

McGough, A. M., and R. Josephs. 1990. On the structure of erythrocyte spectrin in partially expanded membrane skeletons. *Proc. Natl. Acad. Sci. USA.* 87:5208–5212.

Mikrut, J., and R. MacDonald. 1994. Analysis of red blood cell cytoskeleton using an atomic force microscope. *Am. Biotechnol. Lab.* 12:26.

Miyamoto, H., M. Takeuchi, H. Komizu, and A. Kusumi. 1993. Observation of microtubule and cytoskeletal structure by scanning probe microscopy. *Mol. Biol. Cell.* 4:278a.

Mohandas, N., R. Winardi, D. Knowles, A. Leung, M. Parra, E. George, J. Conboy, and J. Chasis. 1992. Molecular basis for membrane rigidity of hereditary ovalocytosis: a novel mechanism involving the cytoplasmic domain of band 3. *J. Clin. Invest.* 89:686–692.

Morrow, J. S., and V. T. Marchesi. 1981. Self-assembly of spectrin oligomers in vitro: a basis for a dynamic cytoskeleton. *J. Cell Biol.* 88:463–468.

Ohno, S., N. Terada, Y. Fujii, H. Ueda, H. Kuramoto, and N. Kamisawa. 1993. Immunocytochemical study of membrane skeletons in abnormally shaped erythrocytes as revealed by a quick-freezing and deep-etching method. *Virchows Arch. A Pathol. Anat.* 422:73–80.

Okabe, A., B. Boots, and K. Sugihara. 1992. Spatial Tessellations: Concepts and Applications of Voronoi Diagrams. John Wiley and Sons, Chichester, England.

Palek, J. 1985. Hereditary elliptocytosis and related disorders. *Clin. Haematol.* 14:45–87.

Palek, J., and P. Jarolim. 1993. Clinical expression and laboratory detection of red blood cell membrane protein mutations. *Semin. Hematol.* 30: 249–283.

Palek, J., and S. Lambert. 1990. Genetics of the red cell membrane skeleton. *Semin. Hematol.* 27:290–332.

Parry, D. A. D., T. W. Dixon, and C. Cohen. 1992. Analysis of the three-alpha-helix motif in the spectrin superfamily of proteins. *Biophys. J.* 61:858–867.

Paulitschke, M., G. B. Nash, D. J. Anstee, M. J. A. Tanner, and W. B. Gratzer. 1995. Perturbation of red blood cell membrane rigidity by extracellular ligands. *Blood.* 86:342–348.

Rakow, A. L., and R. M. Hochmuth. 1975. Effect of heat treatment on the elasticity of human erythrocyte membrane. *Biophys. J.* 15:1095–1100.

Sahr, K. E., T. L. Coetzer, L. S. Moy, L. H. Derick, A. H. Chishti, P. Jarolim, F. Lorenzo, E. Miraglia del Giudice, A. Iolascon, R. Gallanello, A. Cao, J. Delaunay, S.-C. Liu, and J. Palek. 1993. Spectrin Cagliari: an Ala→Gly substitution in helix 1 of beta spectrin repeat 17 that severely disrupts the structure and self-association of the erythrocyte spectrin heterodimer. *J. Biol. Chem.* 268:22656–22662.

Savvides, P., O. Shalev, K. M. John, and S. E. Lux. 1993. Combined spectrin and ankyrin deficiency is common in autosomal dominant hereditary spherocytosis. *Blood.* 82:2953–2960.

Schofield, A. E., D. M. Reardon, and M. J. A. Tanner. 1992a. Defective anion transport activity of the abnormal band 3 in hereditary ovalocytic red blood cells. *Nature.* 355:836–838.

Schofield, A. E., M. J. A. Tanner, J. C. Pinder, B. Clough, P. M. Bayley, G. B. Nash, A. R. Dluzewski, D. M. Reardon, T. M. Cox, R. J. M. Wilson, and W. B. Gratzer. 1992b. Basis of unique red cell membrane properties in hereditary ovalocytosis. *J. Mol. Biol.* 223:949–958.

Schwartz, R. S., J. W. Madsen, A. C. Rybicki, and R. L. Nagel. 1991. Oxidation of spectrin and deformability defects in diabetic erythrocytes. *Diabetes.* 40:701–708.

Scott, M. D., P. Rouyer-Fessard, B. H. Lubin, and Y. Beuzard. 1990. Entrapment of purified alpha-hemoglobin chains in normal erythrocytes: a model for beta-thalassemia. *J. Biol. Chem.* 265:17953–17959.

Shen, B. 1989. Ultrastructure and function of membrane skeleton. *In* Red Blood Cell Membranes: Structure, Function, Clinical Implications. Marcel Dekker, New York. 261–297.

Shen, B. W., R. Josephs, and T. L. Steck. 1986. Ultrastructure of the intact skeleton of the human erythrocyte membrane. *J. Cell Biol.* 102: 997–1006.

Speicher, D. W., and V. Marchesi. 1984. Erythrocyte spectrin is comprised of many homologous triple helical segments. *Nature.* 311:177–180.

Stokke, B., A. Mikkelsen, and A. Elgsaeter. 1986. The human erythrocyte membrane skeleton may be an ionic gel. I. Membrane mechanochemical properties. *Eur. Biophys. J.* 13:203–218.

Tilley, L., G. B. Nash, G. L. Jones, and W. H. Sawyer. 1991. Decreased rotational diffusion of band 3 in Melanesian ovalocytes from Papua, New Guinea. *J. Membr. Biol.* 121:59–66.

Ursitti, J., D. Pumplin, J. Wade, and R. Bloch. 1991. Ultrastructure of the human erythrocyte cytoskeleton and its attachment to the membrane. *Cell Motil. Cytoskeleton.* 19:227–243.

Ursitti, J., and J. Wade. 1993. Ultrastructure and immunocytochemistry of the isolated human erythrocyte membrane skeleton. *Cell Motil. Cytoskeleton.* 25:30–42.

Waugh, R. E. 1983. Effects of abnormal cytoskeletal structure on erythrocyte membrane mechanical properties. *Cell Motility.* 3:609–622.

Waugh, R. E. 1987. Effects of inherited membrane abnormalities on the viscoelastic properties of erythrocyte membrane. *Biophys. J.* 51: 363–369.

Waugh, R. E., and P. Agre. 1988. Reductions of erythrocyte membrane viscoelastic coefficients reflect spectrin deficiencies in hereditary spherocytosis. *J. Clin. Invest.* 81:133–141.

Waugh, R., and E. A. Evans. 1979. Thermoelasticity of red blood cell membrane. *Biophys. J.* 26:115–132.

Yan, Y., E. Winograd, A. Viel, T. Cronin, S. Harrison, and D. Branton. 1993. Crystal structure of the repetitive segments of spectrin. *Science.* 262:2027–2030.